Modified Series and Tapped Switched-Coupled-Inductors Quasi-Z-Source Networks

Saeed Sharifi and Mohammad Monfared, *Senior Member, IEEE*

***Abstract*—This paper proposes two coupled-inductors-based Z-source networks, called the modified series and tapped switched-coupled-inductors quasi-Z-source networks (mSSCL-qZSN and mTSCL-qZSN, respectively). These networks offer high voltage gains with less-than-unity winding turn ratios ($n < 1$), resulting in a reduced inductive element size. Other advantages include a less number of active components and their lower ratings and a higher efficiency. In addition, a lower magnetic core size is required for the proposed ZSNs due to the lower peak magnetizing current. The performance principles and detailed comparative analysis are provided and confirmed through experiments on a 200-W dc–dc converter.**

***Index Terms*—High gain, switched inductors, turn ratio, Z-source networks (ZSNs).**

I. Introduction

THE concept of a Z-source network (ZSN) was first proposed in [1] and [2] as an X-shaped form of inductors and capacitors, providing voltage boost ability to a conventional voltage source inverter. A conventional ZSN has some severe drawbacks, including a low voltage gain, high stresses of circuit components, no common grounds between the input and output, and a high inrush current.

As an enhancement of the conventional ZSN, the quasi-Z-source network (qZSN) was introduced in [3], which could successfully tackle some of the aforementioned drawbacks, while its voltage gain is still too low to be attractive for many applications that require high step-up voltage gains, especially photovoltaic (PVs) and fuel cells. The ZSNs of [4]–[11] attempt to increase the voltage gain of the main converter by employing different step-up Z-source circuits for specific applications. The most recent advancement in this field is the integration of the transformers and coupled inductors in the ZSNs in order to obtain much higher voltage gains. Some of the most successful solutions include the trans-Z (TZ) source [12], the improved trans-Z source [13], the TZ source [14], the (flipped)Γ source [15], [16], the A source [17], and the (q)Y source [18], [19]. In the aforementioned topologies, higher winding turn ratios for obtaining higher gains not only make the design of the inductive elements very difficult but also drastically increase the converter size, weight, and cost. Therefore, the switched inductors/capacitors (SLs/SCs) are integrated with the coupled inductors in [20], which offers a strong boost network, called the switched-coupled-inductors quasi-Z-source network (SCL-qZSN).

Another type of ZSNs is the quasi-switched-boost network (qSBN), which is already proposed in [21]. The qSBN adds a switch and a diode to the conventional ZSN in order to reduce the number of passive components. A class of novel ZSNs, based on the qSBN, have recently been proposed in [22], which utilize two reformed SCL cells, called the series SCL (SSCL) and the tapped SCL (TSCL). These topologies employ coupled inductors, with less-than-unity winding turn ratios ($n < 1$), which significantly reduces the passive components' size. However, both SSCL-qSBN and TSCL-qSBN already suffer from some drawbacks, including a quasi-continuous input current, lack of a common ground between the input and output, relatively high total voltage stresses, and low efficiency.

In order to extract the maximum benefits out of the recently proposed qSBN-based circuit capabilities, this paper proposes modified versions of the SSCL-qSBN and TSCL-qSBN of [22], called modified-SSCL qZSN and modified-TSCL qZSN (mSSCL-qZSN and mTSCL-qZSN, respectively). These networks provide remarkably high voltage gains along with offering a smooth input current, a common ground, and a high conversion efficiency. Also, both the proposed qZSNs allow smaller inductive elements and lower ratings for the switching devices compared to the SSCL-qSBN and the TSCL-qSBN. Moreover, the operation with less-than-unity winding turn ratios ($n < 1$) is possible with the proposed networks, which decreases the current handling requirements of the inductive elements. This also allows us to use a smaller size magnetic core for practical implementation of the inductive elements of the proposed qZSNs. The steady-state performance is analyzed and then verified through a real implementation as a 200-W dc–dc prototype converter. It should be noted that just for the sake of simplicity, the proposed qZSNs are studied within a simple conventional dc–dc converter, and there is almost no limit

Manuscript received May 5, 2018; revised August 1, 2018; accepted September 2, 2018. Date of publication September 26, 2018; date of current version March 29, 2019. *(Corresponding author: Mohammad Monfared.)*

The authors are with the Department of Electrical Engineering, Faculty of Engineering, Ferdowsi University of Mashhad, Mashhad 91779-48974, Iran (e-mail: saeed.sharifi@mail.um.ac.ir; m.monfared@um.ac.ir).

Color versions of one or more of the figures in this paper are available online at http://ieeexplore.ieee.org.

Digital Object Identifier 10.1109/TIE.2018.2870364

0278-0046 © 2018 IEEE. Personal use is permitted, but republication/redistribution requires IEEE permission.
See http://www.ieee.org/publications_standards/publications/rights/index.html for more information.

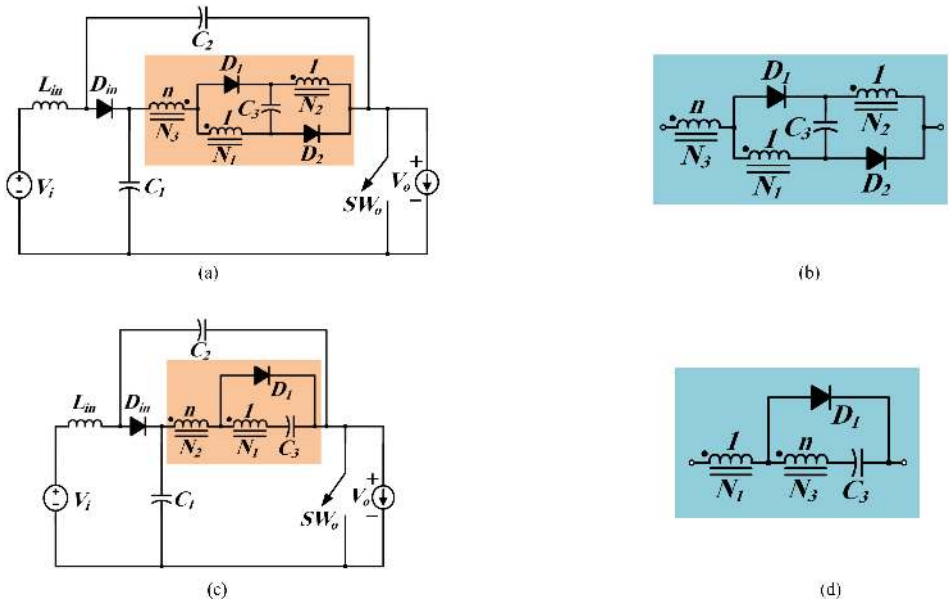

Fig. 1. Modified ZSNs and their original cells. (a) mSSCL-qZSN derived from the (b) SSCL cell of [22] and (c) mTSCL-qZSN derived from the (d) TSCL cell of [22], integrated within the qZSN.

for the applicability of the proposed qZSNs to other converter topologies.

The main properties of both the proposed qZSNs are presented and then compared with their original topologies, confirming their superiority.

II. Proposed qZSNs

Fig. 1(a) and (c) shows the proposed circuit configurations. As already stated, the mSSCL cell of the proposed mSSCL-qZSN is derived from the SSCL cell recently presented in [22] by reversing the coupling polarity of the third winding. Also, the mTSCL cell of the proposed mTSCL-qZSN is a modified version of the TSCL cell of [22] obtained by interchanging the two windings.

A. Operation Principles

The equivalent circuits of the shoot-through (ST) and the non-shoot-through (non-ST) states are considered for the performance analysis, as shown in Fig. 2(a)–(d).

1) mSSCL-qZSN: The performance operation of this qZSN is analyzed by considering equivalent circuits shown in Fig. 2(a) and (b).

a) ST state: As shown in Fig. 2(a), the diodes D_1 and D_2, and the switch SW_o conduct simultaneously. In contrast, the diode D_{in} blocks the current of the capacitor C_1, which charges the mSSCL cell. Also, the input inductor L_{in} is charged by the input voltage and the capacitor C_2. The voltage equations in this state are

$$V_{\text{Lin}} = V_{C_2} + V_i \tag{1}$$

$$V_{N_1} - V_{N_3} = V_{C_1} \tag{2}$$

$$V_{N_3} = nV_{N_1} \tag{3}$$

$$V_{N_1} = V_{C_3} = \frac{V_{C_1}}{1-n}. \tag{4}$$

b) Non-ST state: The switch SW_o turns OFF and the current source models the load, as shown in Fig. 2(b). In this state, the diode D_{in} begins conducting, while the diodes D_1 and D_2 start blocking, as shown in Fig. 2(b). The input voltage charges the capacitor C_1 through L_{in}. In addition, the capacitor C_3 discharges its stored energy into the load in series connection with three coupled windings. It can be written as

$$V_{L_{\text{in}}} = V_o - V_i - V_{C_2} \tag{5}$$

$$V_{N_1} = \frac{V_{C_2} - V_{C_3}}{(2-n)} \tag{6}$$

$$V_{N_1} = \frac{V_o - (2-n)V_{C_3}}{(2-n)}. \tag{7}$$

By applying the volt–second balances on the voltage across the winding N_1 as well as the voltage across the input inductor L_{in}, the steady-state output voltage V_o and voltages across the capacitors C_1, C_2, and C_3 for the mSSCL-qZSN are then obtained from (1)–(7) as

$$G = \frac{V_o}{V_i} = \frac{1 + \frac{1}{(1-n)}}{1 - (2 + \frac{1}{1-n})D} \tag{8}$$

$$V_{C_1} = \frac{(1-n)(1-D)}{(2-n)}V_o \tag{9}$$

$$V_{C_2} = \frac{(D(1-n)+1)}{(2-n)}V_o \tag{10}$$

$$V_{C_3} = \frac{1}{(1-n)}V_{C_1} \tag{11}$$

where D is the ST duty cycle.

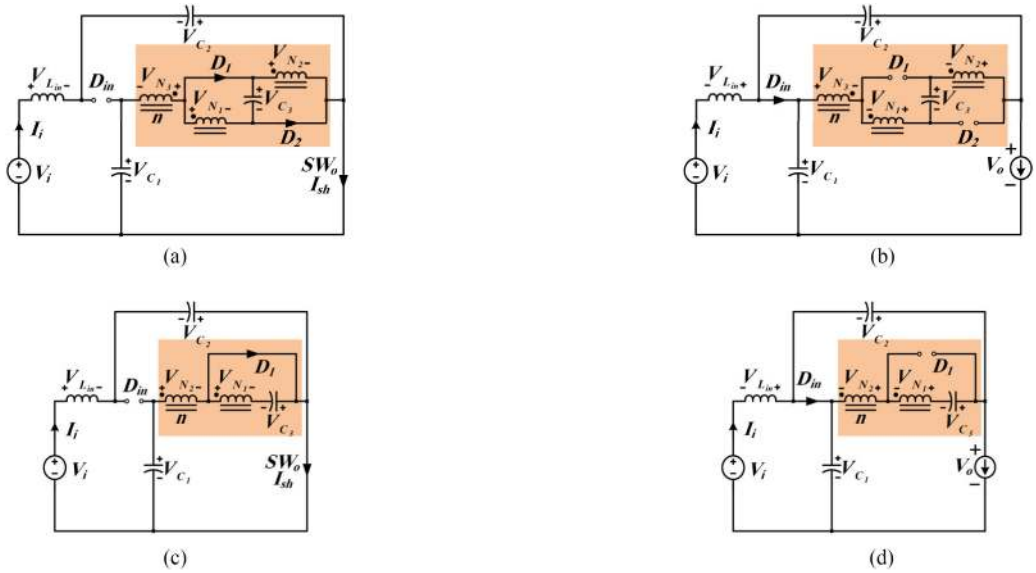

Fig. 2. Operating states. (a) ST and (b) non-ST of mSSCL-qZSN. (c) ST and (d) non-ST of mTSCL-qZSN.

2) mTSCL-qZSN:

a) ST state: Following a similar approach to the previous circuit, from Fig. 2(c) one can readily obtain

$$V_{L_{\text{in}}} = V_{C_2} + V_i \tag{12}$$

$$V_{N_2} = V_{C_1} = nV_{N_1} \tag{13}$$

$$V_{N_1} = V_{C_3} = \frac{V_{C_1}}{n}. \tag{14}$$

b) Non-ST state: Considering Fig. 2(d), the voltage equations are

$$V_{L_{\text{in}}} = V_o - V_i - V_{C_2} \tag{15}$$

$$V_{N_1} = \frac{V_{C_2} - V_{C_3}}{(1+n)} \tag{16}$$

$$V_{N_1} = \frac{V_o - (1+n)V_{C_3}}{(1+n)}. \tag{17}$$

Finally, the same procedure as that for the mSSCL-qZSN is followed to obtain the following results:

$$G = \frac{V_o}{V_i} = \frac{(1+\frac{1}{n})}{1-(2+\frac{1}{n})D} \tag{18}$$

$$V_{C_1} = \frac{n(1-D)}{(1+n)}V_o \tag{19}$$

$$V_{C_2} = \frac{(nD+1)}{(1+n)}V_o \tag{20}$$

$$V_{C_3} = \frac{1}{n}V_{C_1}. \tag{21}$$

The voltage-gain equations of the proposed qZSNs already derived in (8) and (18) are reported in Table I. In addition, the voltage-gain equations of the SSCL-qSBN, TSCL-qSBN, and SCL-qZSN with an introducing cell factor (CF) are also given in this table. The introduction of CF, as defined in this table, allows us to achieve a same voltage gain for all ZSNs under study only by a proper selection of the winding turn ratio such that the same CF is obtained for all networks. According to (8) and (18), high step-up voltage gains for both the proposed qZSNs are possible with a less-than-unity winding turn ratio $(n < 1)$. The SSCL-qSBN and TSCL-qSBN of [22] also benefit from the same feature. Fig. 3(a) and (b) compares the voltage gain profile of the proposed qZSNs with that of their originals, where G is the ratio of the output to the input voltage (the voltage gain). According to these figures, for the winding turn ratios closer to unity $(n \sim 1)$, the mSSCL-qZSN offers a higher gain, which also holds for the TSCL-qSBN. In contrast, for much lower than unity turn ratios $(n \sim 0)$, the mTSCL-qZSN offers a higher gain than the SSCL-qSBN, which can be readily concluded from (18). Besides, the SCL-qZSN requires a high winding turn ratio $(n > 1)$ to achieve the same voltage gain as others.

III. Component Parameter Design and Comparison

The component requirements of the proposed qZSNs, such as the number of semiconductors and their ratings, and the total cell inductances and their sizes, are all investigated in this section and the results are presented in Figs. 4–6 and Table II.

A. Inductive Elements

1) Magnetizing Inductance (L_m): Considering the maximum tolerable ripple of the magnetizing current (I_m) to be $\alpha\%$, the required magnetizing inductance (L_m) can be obtained as

$$L_m = \frac{V_{N1}DT_{sw}}{\alpha\%I_m} \tag{22}$$

where V_{N1} and T_{sw} are the peak voltage across the winding N_1 during the ST state and the switching period, respectively.

The magnetizing inductance of the proposed Z-source cells is calculated in terms of the voltage gain (G), winding turn ratio,

TABLE I
VOLTAGE GAIN EQUATIONS FOR THE PROPOSED AND CONVENTIONAL ZSNS

Voltage Gain (G) / Cell Factor (CF)	SSCL-qSBN [22]	TSCL-qSBN [22]	SCL-qZSN [20]	Proposed Z-source Networks	
				mSSCL-qZSN	mTSCL-qZSN
$\frac{1+CF}{1-(2+CF)D}$	$\left(\frac{2}{n}\right)$; $n<1$	$\left(\frac{2}{1/n-1}\right)$; $n<1$	$(1+n)$; $n>0$	$\left(\frac{1}{1-n}\right)$; $n<1$	$\left(\frac{1}{n}\right)$; $n<1$

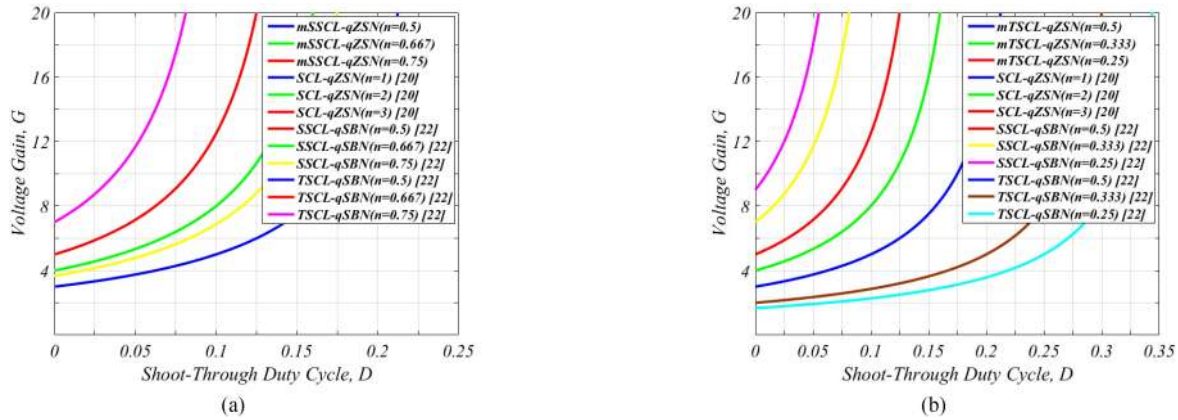

Fig. 3. Comparative plot of the gain versus shoot-through duty cycle among the proposed (a) mSSCL-qZSN, (b) mTSCL-qZSN, and the competitors.

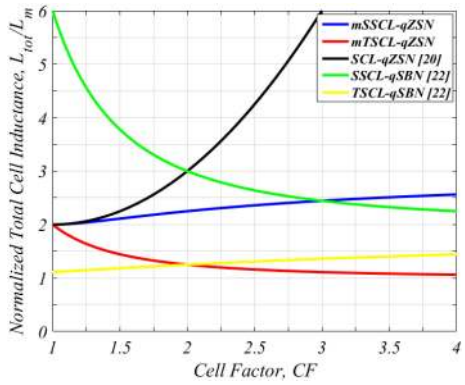

Fig. 4. Normalized total cell inductance versus the cell factor CF.

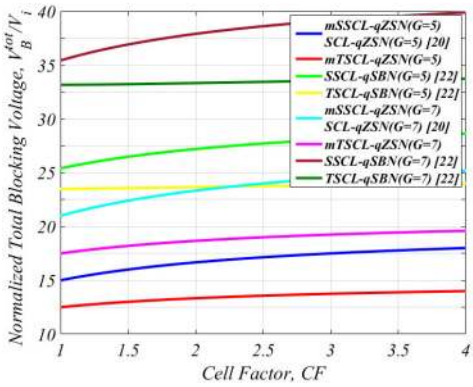

Fig. 6. Comparison of the normalized total blocking voltage of semiconductors.

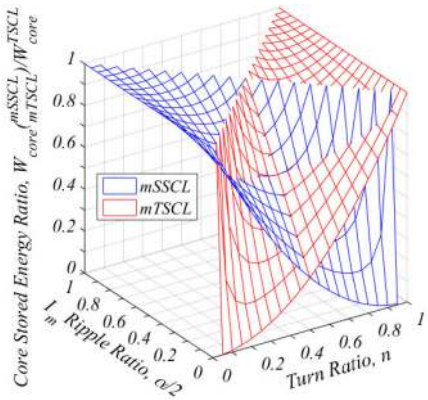

Fig. 5. Core stored energy ratio of the mSSCL and mTSCL cells.

and cell factor (CF) as follows:

$$L_m^{\mathrm{mSSCL}} = \frac{n^2}{(1-n)^2} L_m^{\mathrm{mTSCL}} = \frac{(G+1)(G-1-CF)}{(1-n)^2 G(2+CF)^2} \times L_m^B \tag{23}$$

where

$$L_m^B = \frac{V_i^2}{\alpha\% f_{sw} P_o} \tag{24}$$

and P_o and V_i are the rated output power and the input voltage, respectively.

In addition, the total cell inductance (L_{tot}) for both the proposed qZSNs is calculated as the sum of all inductances of the cell windings. Thus, neglecting the leakage inductances, it can

TABLE II
COMPARISON OF THE NUMBER OF PASSIVE AND ACTIVE COMPONENTS

Components		Z-Source Impedance Networks				
		SSCL-qSBN [22]	TSCL-qSBN [22]	SCL-qZSN [20]	Proposed mSSCL-qZSN	Proposed mTSCL-qZSN
No.	Inductors	3 coupled-inductors	2 coupled-inductors	1 inductor and 3 coupled-inductors	1 inductor and 3 coupled-inductors	1 inductor and 2 coupled-inductors
	Capacitors	2	2	3	3	3
	Diodes	4	3	3	3	2
	Switches	1	1	0	0	0
Remarks		• Large inductive element with a relatively large magnetic core. • High current handling requirement of coupled-inductors. • Very high total blocking voltage of semiconductors. • Quasi-continuous input current.	• Small inductive element with a relatively large magnetic core. • Moderate current handling requirement of coupled-inductors. • High total blocking voltage of semiconductors. • Quasi-continuous input current.	• Very large inductive element with a relatively large magnetic core. • Moderate current handling requirement of coupled-inductors. • Low total blocking voltage of semiconductors. • Continuous input current. • Common ground between input and output.	• Small inductive element with a small magnetic core. • Low current handling requirement of coupled-inductors. • Low total blocking voltage of semiconductors. • Continuous input current. • Common ground between input and output.	• Very small inductive element with a small magnetic core. • Low current handling requirement of coupled-inductors. • Very low total blocking voltage of semiconductors. • Continuous input current. • Common ground between input and output.

be written as

$$L_{\text{tot}}^{\text{mSSCL}} = L_m^{\text{mSSCL}}(2+n^2)\ ;\ n = 1 - \frac{1}{CF} \tag{25}$$

$$L_{\text{tot}}^{\text{mTSCL}} = L_m^{\text{mTSCL}}(1+n^2)\ ;\ n = \frac{1}{CF}. \tag{26}$$

By assuming the same magnetizing inductance (L_m) for both the proposed Z-source cells and other competitors, the normalized total cell inductances are compared, as shown in Fig. 4. This figure shows that the total cell-inductance requirement of the SCL-qZSN increases exponentially with increase in CF. Obviously, the proposed qZSNs need a lower total cell inductance than the SCL-qZSN for all CFs leading to the smaller inductive elements. In addition, for the mSSCL-qZSN, the total cell inductance is lower than that for the SSCL-qSBN with $CF < 3$ while being slightly higher for $CF > 3$. Interestingly, both TSCL-qSBN and mTSCL-qZSN have much lower inductance requirements compared to other networks. In addition, for $CF > 2$, the mTSCL-qZSN requires the lowest total cell inductance among all ZSNs. These features are achieved by the advantage of a possibility of less-than-unity winding turn ratios required for a same voltage gain.

2) Magnetizing Current (I_m): Similar to the magnetizing inductance, the magnetizing current of the coupled inductors is referred to the primary winding (N_1). From the non-ST state of the proposed qZSNs shown in Fig. 2(b) and (d), it can be written as

$$I_m^{\text{mSSCL}} = (1-n)(1+CF)I_{N_3}^{\text{NST}} \tag{27}$$

$$I_m^{\text{mTSCL}} = n(1+CF)I_{N_2}^{\text{NST}}. \tag{28}$$

Considering the series connection of the windings in this state and applying the current–second balance on the current of the capacitor C_2 and assuming that I_i is the input current, one obtains

$$I_{N_1}^{\text{NST}} = I_{N_2}^{\text{NST}} = I_{N_3}^{\text{NST}} = \frac{1}{1+CF} I_i. \tag{29}$$

Thus, we have

$$I_m^{\text{mSSCL}} = (1-n)I_i \tag{30}$$

$$I_m^{\text{mTSCL}} = nI_i. \tag{31}$$

According to (30) and (31), with less-than-unity winding turn ratios, the magnetizing current is lower than the input current for both the proposed qZSNs. It should be noted that for any winding turn ratio, the magnetizing current of the coupled inductors of the TSCL-qSBN is always equal to the input current, while it is more than that for the SSCL-qSBN. In other words, the proposed qZSNs offer high voltage gains with less-than-unity winding turn ratios, which reduces the current-handling requirement of the coupled inductors of the Z-source cells.

3) Magnetic Core Size of the Cells: In [23], the core size of the coupled inductors is evaluated by the peak stored energy in the core. Assuming the same magnetizing inductance (L_m) for all ZSNs, the peak stored energy in the core is characterized by

$$W_{\text{Core}} \propto I_{m\_\max}^2 \tag{32}$$

where $I_{m\_\max}$ is the peak magnetizing current of the coupled inductors.

The TSCL-qSBN and SCL-qZSN produce the same yet lower peak magnetizing current than the SSCL-qSBN. Thus, for the magnetic core size comparison, the ratio of the core stored energy of the proposed Z-source cells to the core stored energy of the TSCL cell or the SCL cell is evaluated as

$$\frac{W_{core}^{\text{mSSCL}}}{W_{\text{core}}^{\text{mTSCL}}} = \frac{\left(I_{m\_\max}^{\text{mSSCL}}\right)^2}{\left(I_{m\_\max}^{\text{mTSCL}}\right)^2} = \left(\frac{\left(\frac{1}{CF}\right) + (CF) \times \frac{\alpha\%}{2}}{1+\frac{\alpha\%}{2}}\right)^2 \tag{33}$$

where $\alpha\%$ is the maximum tolerable ripple of I_m.

Equation (33) is obtained by assuming the same input voltage, output power, and switching frequency.

Assuming

$$\frac{\alpha\%}{2} < 100\% \tag{34}$$

the previous equation (33) can be plotted as a function of $\alpha/2$ and the winding turn ratio, as shown in Fig. 5. Obviously, for any specific magnetizing current ripple, by a proper selection of the winding turn ratio from this figure, the core stored energy of both the proposed Z-source cells can be lower than that of the TSCL(SCL) cell. In other words, for any winding turn ratio, there is an I_m current ripple that ensures reducing the stored energy in the core of the mSSCL and mTSCL cells below the TSCL(SCL)-cell requirement. Consequently, this current ripple determines the proper magnetizing inductance (L_m) for the proposed Z-source cells.

As a general design method considering Fig. 4, the proper CF for each of the proposed qZSNs can be selected so as to minimize the total cell-inductance requirement. Then, this cell factor can be translated into its corresponding winding turn ratio and then the magnetizing current ripple using Fig. 5, which leads to a lower core stored energy, and thus into a smaller magnetic core size compared to the SSCL-qSBN, TSCL-qSBN, and SCL-qZSN.

4) Input Inductance (L_{in}): The input inductance is calculated by using the same equation as that for the magnetizing inductance. Thus, with $\beta\%$ as the tolerable input current ripple, the input inductance of both the proposed qZSNs is obtained as

$$L_{\text{in}} = \frac{(G-1-CF)(1+G)(1+CF)}{G(2+CF)^2} \times \frac{V_i^2}{\beta\% f_{sw} P_o}. \tag{35}$$

B. Capacitive Elements

The capacitor design is based on the maximum allowable voltage ripple. The time duration and the amplitude of the current flowing through the capacitors in each state of operation define this constraint. Assuming $\gamma\%$ as the maximum tolerable capacitor voltage ripple and considering their current being in the ST state, the following equations define the required capacitors for the proposed qZSNs:

$$C_1 = \frac{G-1+CF(G(2+CF)-1)}{G(G(1+CF)+1)} \times C_B \tag{36}$$

$$C_2 = \frac{(G-CF-1)}{G(G(1+CF)-1)} \times C_B \tag{37}$$

$$C_3^{\text{mSSCL}} = \frac{(1-n)}{n} C_3^{\text{mTSCL}} = \frac{(1-n)}{G} \times C_B \tag{38}$$

where

$$C_B = \frac{P_o}{\gamma\% f_{sw} V_i^2}. \tag{39}$$

C. Switch and Diode Blocking Voltages

The blocking voltages of the switching devices for the proposed qZSNs are obtained as follows:

$$V_{D\text{in}} = V_{SW\,o} = GV_i \tag{40}$$

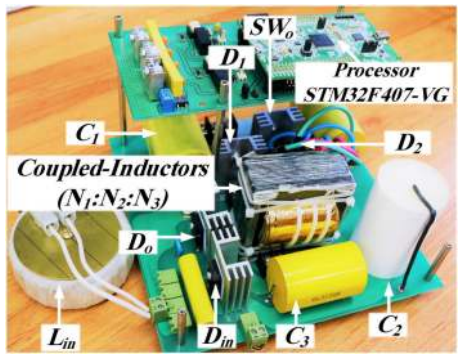

Fig. 7. DC–DC prototype picture.

TABLE III
EXPERIMENTAL PARAMETERS

Description	Values
Rated Power	200W
Input Voltage	$40V_{dc}$
Output Voltage	$200V_{dc}$
Frequency, f_{sw} & Duty Cycle, D	10kHz, 0.1
Capacitances: C_1, C_2, C_3, C_o	130μF, 50μF, 48μF, 20μF
Input inductance, L_{in}	630μH
Magnetizing Inductance (L_m):	250μH
mSSCL-cell (N_1:N_2:N_3→n)	(12:12:6→n=0.5)
mTSCL-cell (N_1:N_2→n)	(12:6→n=0.5)

$$V_{D_1,D_2}^{\text{mSSCL}} = \frac{G}{(1-n)(1+CF)} V_i \tag{41}$$

$$V_{D_1}^{\text{mTSCL}} = \frac{G}{n(1+CF)} V_i. \tag{42}$$

In order to compare the voltage stresses, the normalized total blocking voltage based on the input voltage V_i is calculated from the sum of (40)–(42) and the result is plotted in Fig. 6 for each of the proposed qZSNs. This parameter is also plotted for the SSCL-qSBN, TSCL-qSBN, and SCL-qZSN in this figure. As seen, for the same voltage gain and CF, the total blocking voltage of the switching devices for both the proposed qZSNs is lower than that of both SSCL-qSBN and TSCL-qSBN. Thus, lower ratings for the semiconductor switches and diodes can be ensured, leading to lower power losses and implementation costs. In addition, the total blocking voltage of the mSSCL-qZSN (mTSCL-qZSN) is the same as (lower than) that of the SCL-qZSN.

Finally, the number of passive and active components and some conclusions about the circuit requirements, based on the previous results, are presented in Table II.

IV. PERFORMANCE EVALUATION

In order to verify the principles of steady-state operation and the properties of the proposed qZSNs, both networks are implemented as a conventional boost dc–dc converter. The experimental setup is shown in Fig. 7. The prototype parameters are summarized in Table III. The ARM microcontroller STM32F407VG is used to generate the constant pulsewidth gating signal of the

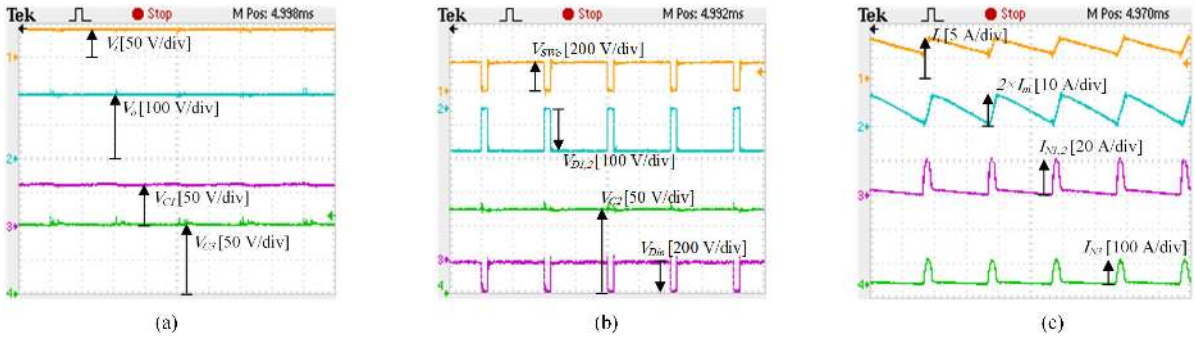

Fig. 8. mSSCL-qZSN experimental waveforms. (a) Input, output, and the capacitors C_1 and C_3 voltages. (b) Voltages across the switch SW_o, diodes $D_{1,2}$ and D_{in}, and capacitor C_2. (c) Input, magnetizing, and the windings N_1, N_2, and N_3 currents.

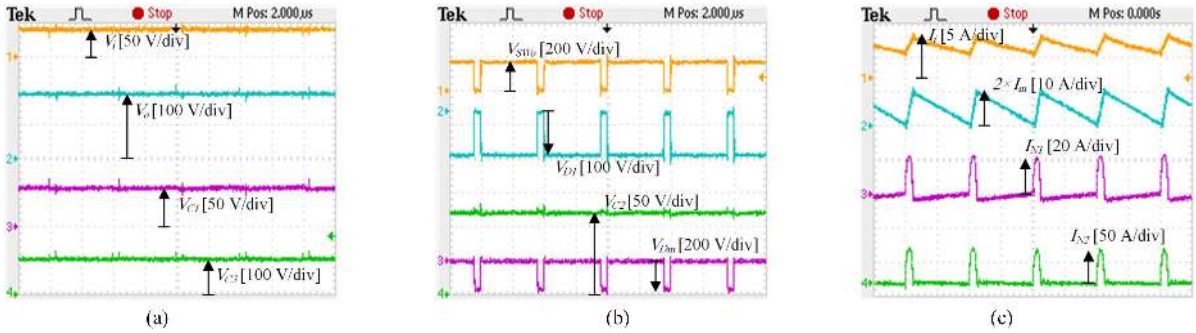

Fig. 9. mTSCL-qZSN experimental waveforms. (a) Input, output, and the capacitors C_1 and C_3 voltages. (b) Voltages across the switch SW_o, diodes D_1 and D_{in}, and capacitor C_2. (c) Input, magnetizing, and the windings N_1 and N_2 currents.

switch SW_o. The duty cycle $D = 0.1$ is used for both the proposed topologies. According to the windings turn ratios given in Table III and the voltage-gain equations already derived in Section II, this duty cycle results in a voltage gain of $G = 5$ for both topologies. The theoretical output voltage and the voltages across the capacitors C_1, C_2, and C_3 are calculated as $200V_{\text{dc}}$, $60V_{\text{dc}}$, $140V_{\text{dc}}$, and $120V_{\text{dc}}$, respectively, for both topologies. It should also be noted that the inductive element of the proposed Z-source cells is fabricated using copper foils wound on an EE ferrite magnetic core to reduce the leakage inductance of the coupled inductors.

The experimental waveforms of the proposed mSSCL-qZSN and mTSCL-qZSN are shown in Figs. 8 and 9, respectively. The input voltage of $40V_{\text{dc}}$ is boosted to $191V_{\text{dc}}$ and $193V_{\text{dc}}$ for the mSSCL-qZSN and the mTSCL-qZSN, respectively. This is in close agreement with the expected theoretical values calculated earlier as $200V_{\text{dc}}$. The slight decrease in the output voltage compared to the calculated value can be attributed to the parasitic resistances and the ON-state voltage drops across the semiconductor switch and diodes.

From the voltage waveforms of the switch SW_o, and the diodes $D_{1(,2)}$ and D_{in}, one can find that, as already expected, SW_o and D_1 and/or D_2 are turned ON and conduct during the shoot-through state, while D_{in} is blocking. The voltage-blocking values of all semiconductors can be simply verified by (40)–(42), considering the waveforms shown in Figs. 8(b) and 9(b).

The current waveforms confirm that the input current is continuous, which can be considered as a major improvement over the qSBN-based competitors of [22] that produce quasi-continuous input currents. The ripple of the input current is mainly determined by the input inductor. According to (35), by designing the input inductor as $L_{\text{in}} = 630\,\mu$H, the input current ripple is about 57%, which is in good agreement with the experimental waveforms. The magnetizing currents of both the proposed Z-source cells are referred to the primary winding and then measured by multiplying the winding currents with their turn numbers, i.e., $N_1 I_m = N_1 I_{N1} + N_2 I_{N2} (+N_3 I_{N3})$, which can be simplified as $2I_m = 2I_{N1} + 2I_{N2} + I_{N3}$ for the mSSCL cell and $2I_m = 2I_{N1} + I_{N2}$ for the mTSCL cell. Thus, the waveforms of the magnetizing currents are measured as twice their real values. The experimental waveforms show that the magnetizing currents oscillate from slightly higher than zero to almost twice their average values, which confirms (23). Also, both (30) and (31), which relate the magnetizing and input currents, can be confirmed with the magnetizing currents given in Figs. 8(c) and 9(c), where the average values of I_{m} are measured as half of the average input currents because of the winding turn ratio selection as $n = 0.5$.

It is worth mentioning that a sinusoidal positive half-cycle resonance appears in the cell-winding currents during the shoot-through state, as shown in Figs. 8(c) and 9(c). By a proper selection of the capacitances C_1 and C_3 such that this resonance can be completed before the end of the shoot-through state, the voltage spikes across the switching devices are significantly reduced.

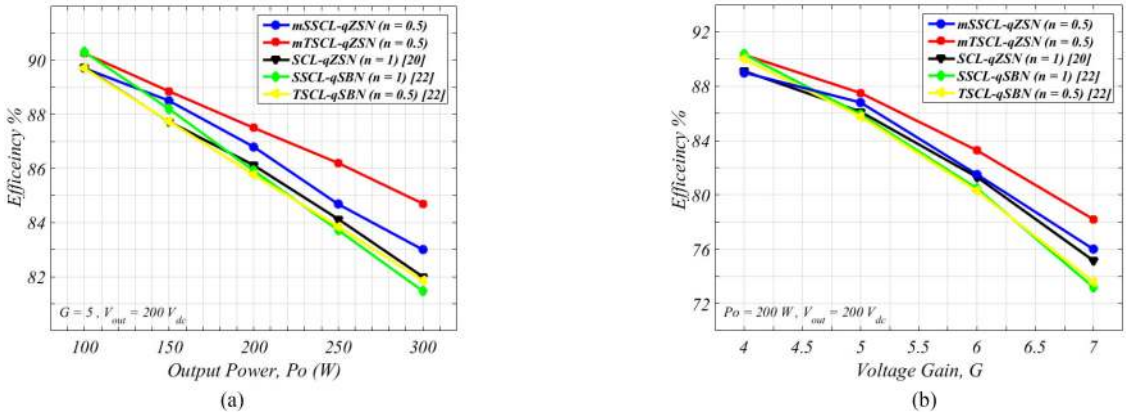

Fig. 10. Measured efficiency comparison with (a) output power variation for constant output voltage and gain, and (b) voltage gain variation for constant output voltage and power.

TABLE IV
MEASURED AND CALCULATED PARAMETER VALUES

Parameters ($V_i = 40V_{dc}$)		mSSCL-qZSN	mTSCL-qZSN
V_o	*Measurement*	$191V_{dc}$	$193V_{dc}$
	Calculation	$200V_{dc}$	$200V_{dc}$
V_{C1}	*Measurement*	$56V_{dc}$	$58V_{dc}$
	Calculation	$60V_{dc}$	$60V_{dc}$
V_{C2}	*Measurement*	$125V_{dc}$	$123V_{dc}$
	Calculation	$140V_{dc}$	$140V_{dc}$
V_{C3}	*Measurement*	$108V_{dc}$	$112V_{dc}$
	Calculation	$120V_{dc}$	$120V_{dc}$
I_i	*Measurement*	5.5A	5.3A
	Calculation	5A	5A
I_m	*Measurement*	2.78A	2.67A
	Calculation	2.5 A	2.5A

The quantitative results of the experiments along with the theoretically calculated values for the proposed qZSNs are summarized in Table IV. All calculated values are obtained by neglecting the power loss of the conversion process.

Finally, the measured efficiencies are reported. In the first study, the efficiency as a function of output power is measured with $V_o = 200V_{dc}$ and $G = 5$, as shown in Fig. 10(a). Evidently, the efficiencies of all topologies decrease with increase in power. In addition, the proposed qZSNs offer the highest efficiency, which may be attributed to their lower number of switching devices. However, the efficiency of the mSSCL-qZSN is less than that of the mTSCL-qZSN due to the higher number of windings and larger currents through them.

In another study, the efficiency as a function of voltage gain, with $P_o = 200\,\text{W}$ and $V_o = 200V_{dc}$, is plotted in Fig. 10(b). Again the proposed qZSNs, especially the mTSCL-qZSN, present higher efficiencies than others for different gains.

Regarding the efficiency, among the proposed qZSNs, the mTSCL-qZSN offers higher efficiencies than the mSSCL-qZSN, mainly resulting from its lower winding currents and less number of windings and diodes compared to the mSSCL-qZSN.

V. CONCLUSION

Two modified qZSNs with coupled inductors were proposed in this paper. The most prominent features of the proposed qZSNs can be listed as:

1) a high voltage gain attainable with less-than-unity winding turn ratios ($n < 1$);
2) small inductive elements;
3) low current handling requirements of the coupled inductors;
4) small magnetic core size;
5) low voltage stresses across semiconductors.

All these were obtained by a proper reconfiguration of the SSCL and TSCL cells proposed earlier. The principles of the steady-state operation were analyzed and the theoretical results were then confirmed through experimental tests.

REFERENCES

[1] F. Z. Peng, "Z-source inverter," *IEEE Trans. Ind. Appl.*, vol. 39, no. 2, pp. 504–510, Mar./Apr. 2003.
[2] F. Z. Peng, X. Yuan, X. Fang, and Z. Qian, "Z-source inverter for adjustable speed drives," *IEEE Power Electron. Lett.*, vol. 1, no. 2, pp. 33–35, Jun. 2003.
[3] J. Anderson and F. Z. Peng, "Four quasi-Z-source inverters," in *Proc. IEEE Power Electron. Spec. Conf.*, 2008, pp. 2743–2749.
[4] C. J. Gajanayake, F. L. Luo, H. B. Gooi, P. L. So, and L. K. Siow, "Extended-boost Z-source inverters," *IEEE Trans. Power Electron.*, vol. 25, no. 10, pp. 2642–2652, Oct. 2010.
[5] M. Zhu, K. Yu, and F. L. Luo, "Switched inductor Z-source inverter," *IEEE Trans. Power Electron.*, vol. 25, no. 8, pp. 2150–2158, Aug. 2010.
[6] M.-K. Nguyen, Y.-C. Lim, and G.-B. Cho, "Switched-inductor quasi-Z-source inverter," *IEEE Trans. Power Electron.*, vol. 26, no. 11, pp. 3183–3191, Nov. 2011.
[7] H. Fathi and H. Madadi, "Enhanced-boost Z-source inverters with switched Z-impedance," *IEEE Trans. Ind. Electron.*, vol. 63, no. 2, pp. 691–703, Feb. 2016.
[8] A.-V. Ho, T.-W. Chun, and H.-G. Kim, "Extended boost active-switched-capacitor/switched-inductor quasi-Z-source inverters," *IEEE Trans. Power Electron.*, vol. 30, no. 10, pp. 5681–5690, Oct. 2015.
[9] D. Li, P. C. Loh, M. Zhu, F. Gao, and F. Blaabjerg, "Enhanced-boost Z-source inverters with alternate-cascaded switched- and tapped-inductor cells," *IEEE Trans. Ind. Electron.*, vol. 60, no. 9, pp. 3567–3578, Sep. 2013.
[10] V. Jagan, J. Kotturu, and S. Das, "Enhanced-boost quasi-Z-source inverters with two-switched impedance networks," *IEEE Trans. Ind. Electron.*, vol. 64, no. 9, pp. 6885–6897, Sep. 2017.

[11] S. Sharifi, F. Jahani, and M. Monfared, "Direct single phase ac–ac converters based on novel series impedance networks," *IEEE Trans. Power Electron.*, vol. 33, no. 12, pp. 10380–10389, Dec. 2018.
[12] W. Qian, F. Z. Peng, and H. Cha, "Trans-Z-source inverters," *IEEE Trans. Power Electron.*, vol. 26, no. 12, pp. 3453–3463, Dec. 2011.
[13] M.-K. Nguyen, Y.-C. Lim, and S.-J. Park, "Improved trans-Z-source inverter with continuous input current and boost inversion capability," *IEEE Trans. Power Electron.*, vol. 28, no. 10, pp. 4500–4510, Oct. 2013.
[14] M.-K Nguyen, Y.-C Lim, and Y.-G Kim, "TZ-source inverters," *IEEE Trans. Ind. Electron.*, vol. 60, no. 12, pp. 5686–5695, Dec. 2013.
[15] P. C. Loh, D. Li, and F. Blaabjerg, "Γ-Z-source inverters," *IEEE Trans. Power Electron.*, vol. 28, no. 11, pp. 4880–4884, Nov. 2013.
[16] P. C. Loh and F. Blaabjerg, "Magnetically coupled impedance-source inverters," *IEEE Trans. Ind. Appl.*, vol. 49, no. 5, pp. 2177–2187, Sep./Oct. 2013.
[17] Y. P. Siwakoti, F. Blaabjerg, V. P. Galigekere, A. Ayachit, and M. K. Kazimierczuk, "A-source impedance network," *IEEE Trans. Power Electron.*, vol. 31, no. 12, pp. 8081–8087, Dec. 2016.
[18] Y. P. Siwakoti, P. C. Loh, F. Blaabjerg, S. J. Andreasen, and G. E. Town, "Y-source boost dc/dc converter for distributed generation," *IEEE Trans. Ind. Electron.*, vol. 62, no. 2, pp. 1059–1069, Feb. 2015.
[19] Y. P. Siwakoti, F. Blaabjerg, and P. C. Loh, "Quasi-Y-source boost dc–dc converter," *IEEE Trans. Power Electron.*, vol. 30, no. 12, pp. 6514–6519, Dec. 2015.
[20] H. F. Ahmed, H. Cha, S.-H. Kim, and H.-G. Kim, "Switched-coupled-inductor quasi-Z-source inverter," *IEEE Trans. Power Electron.*, vol. 31, no. 2, pp. 1241–1254, Feb. 2016.
[21] M.-K. Nguyen, T.-V. Le, S.-J. Park, and Y.-C. Lim, "A class of quasi-switched boost inverters," *IEEE Trans. Ind. Electron.*, vol. 62, no. 3, pp. 1526–1536, Mar. 2015.
[22] S. Sharifi and M. Monfared, "Series and tapped switched-coupled-inductors impedance networks," *IEEE Trans. Ind. Electron.*, vol. 65, no. 12, pp. 9498–9508, Dec. 2018.
[23] W. T. Mclyman, *Transformer and Inductor Design Handbook*. Boca Raton, FL, USA: CRC Press, 2011.

Saeed Sharifi received the B.Sc. and M.Sc. degrees (with honors) in electrical engineering from the Ferdowsi University of Mashhad, Mashhad, Iran, in 2015 and 2018, respectively.

His research interests include power electronic converters, especially impedance networks, high-order passive filters, grid-connected converters, and ac–ac converters.

Mohammad Monfared (S'07–M'10–SM'15) received the B.Sc. degree in electrical engineering from the Ferdowsi University of Mashhad, Mashhad, Iran, in 2004, and the M.Sc. and Ph.D. degrees (both with honors) in electrical engineering from the Amirkabir University of Technology, Tehran, Iran, in 2006 and 2010, respectively.

He is currently an Associate Professor with the Ferdowsi University of Mashhad. His research interests include power electronics, renewable energy systems, and power quality.

Dr. Monfared received the Best Researcher Award of the Ferdowsi University of Mashhad in 2015.